Multi-Channel Digital SiPMs: Concept, Analysis and Implementation

Shingo Mandai†, *Student Member, IEEE,* and Edoardo Charbon, *Member, IEEE*

***Abstract*—This paper presents a comprehensive statistical analysis of timing resolution in a digital silicon photomultiplier (D-SiPM) when multi timestamp is available. We look at the effect of dart count rate (DCR) on timing resolution in these devices as compared to analog silicon photomultipliers (A-SiPMs). The analysis includes photon detection efficiency (PDE), DCR, electrical jitter of the detector with a LYSO crystal. Timing resolution is analyzed utilizing a single timestamp or multiple timestamps. Simulation results show that D-SiPMs utilizing multiple timestamps (Multi-channel D-SiPM) can be more tolerant to DCR than those utilizing a single timestamp. The timing resolution is 13%, 20% and 40% better at 1000 detected photons, 200 ps rise time and 40 ns decay time of a LYSO scintillator, without DCR, with 1 MHz DCR and with 10 MHz DCR, respectively. Based on these findings, we propose new architectures to acquire multiple timestamps without sacrificing fill-factor. This paper also includes the implementation and characterization of 4 × 4 Multi-channel D-SiPMs coupled with an array of 44ps LSB TDCs for coincidence detection of gamma rays. The pitch of the SiPMs is 800 µm and the number of pixels in one SiPM is 416. The pixel has a 57 % fill factor with 121 ps timing resolution for a single photon. The SiPM timing resolution for single photon detection is 179 ps FWHM.**

I. Introduction

SIPMS are an alternative to PMTs, often preferred because of their tolerance to magnetic fields, compactness, and low bias voltage [3]–[9]. At least two flavors exist for SiPMs: analog and digital. An analog SiPM (A-SiPM) consists of an array of avalanche photodiodes operating in Geiger mode, whose avalanche currents are summed in one node as shown in Fig. 1 (a) [3]–[8]. The resulting current is proportional to the number of detected photons, thus providing single- and multiple-photon detection capability. In a digital SiPM (D-SiPM), each photo-detecting cell or pixel consists of a single-photon avalanche diode (SPAD), specific circuit elements are added to generate digital signals for each photon detection and to turn off the SPAD when its activity is deemed too high. The SPAD is known in this case as "screamer" [9]. All of the SPAD outputs are combined together by means of a digital OR, see Fig. 1 (b). In most D-SiPMs, the global output is directly routed to an on-chip time-to-digital converter (TDC) to reduce external components and temporal noise. Though, the time uncertainty for single-photon detection is limited by SPAD jitter and TDC non-linearities, as well as systematic skews due to imperfectly balanced routing. A-SiPMs are especially sensitive to these systematic skews, while in D-SiPMs they can be largely removed or compensated. However in D-SiPMs, only one optical photon or noise event determines the response of the sensor. Alternatively, the approach pursued in [10] can achieve balanced routing by implementing a on-pixel TDC as shown in Fig. 1 (c). At the same time multiple photons can be detected independently, thus providing more detailed statistical information of the Gamma event. However, the fill factor is low due to the use of a TDC per pixel.

A better trade-off is the architecture shown in Fig. 1 (d), denominated Multi-channel D-SiPM (MD-SiPM), which shares a number of SPADs per TDC. In this paper, the timing resolution for conventional D-SiPMs and ideal Multi-channel D-SiPMs is discussed based on [11], [12], then, a more realistic analysis for MD-SiPMs including the effects of DCR is presented in section II. The implementation and characterization of the MD-SiPM fabricated in CMOS process is shown in section III. Concluding remarks are presented in section IV

Manuscript received November 16, 2012.

Authors are with TU Delft, The Netherlands (†s.mandai@tudelft.nl)

The research leading to these results has received funding from the European Union Seventh Framework Program under Grant Agreement n°256984 [1], [2]. The authors would like to thank Dr. Yuki Marumaya, Dr. Matthew Fishburn, Chockalingam Veerappan, and Vishwas Jain of TU Delft, Pierre Jarron from CERN. The authors are also grateful to Xilinx, Inc. for FPGA donations.

II. Simulation Model and Results

A. Simulation Model

For the emitted photons from a LYSO scintillator, we can assume that photons are detected with the arrival time, θ. Time information of each photon can be considered as statistically independent and identically distributed (i.i.d.) following a probability density function (pdf), which has been modeled as a double-exponential with rise time t_r and decay time t_d [13] $f(t|\theta) = (\exp(-\frac{t-\theta}{t_d}) - \exp(-\frac{t-\theta}{t_r}))/(t_d - t_r)$ when $t > \theta$, otherwise, $f(t|\theta) = 0$. Upon photon impingement, the SPAD jitter and an electrical jitter are convolved with the scintillator-based pdf, $f_{emi}(t|\theta)$. The DCR follows an exponential probability distribution with event rate, λ, and reset time, t_r, as $f(t) = \lambda \exp(-\lambda(t - t_r))$ when $t > t_r$, otherwise, $f(t) = 0$. The pdf of DCR should also be convolved with electrical jitter, forming DCR-based pdf, $f_{dcr}(t|t_r)$. The detection cycle or frame starts at the earliest before θ and at the latest frame period, T before θ, so the DCR-based pdf is summed up for each reset time and then normalized. The scintillator-based pdf and DCR-based pdf are mixed with mixing ratio $\alpha : (1 - \alpha)$ when α is defined by the percentage of photons emitted from scintillator, N, out of total detectable events, $N + \lambda T$, as below.

$$f_{emi+dcr}(t|\theta) = \alpha f_{emi}(t|\theta) + (1-\alpha)\frac{\int_{\theta-T}^{\theta} f_{dcr}(t|tr)\, dr}{\int_{\theta-T}^{\theta}\int_{t_r}^{\infty} f_{dcr}(t|tr)\, dt\, dr} \quad (1)$$

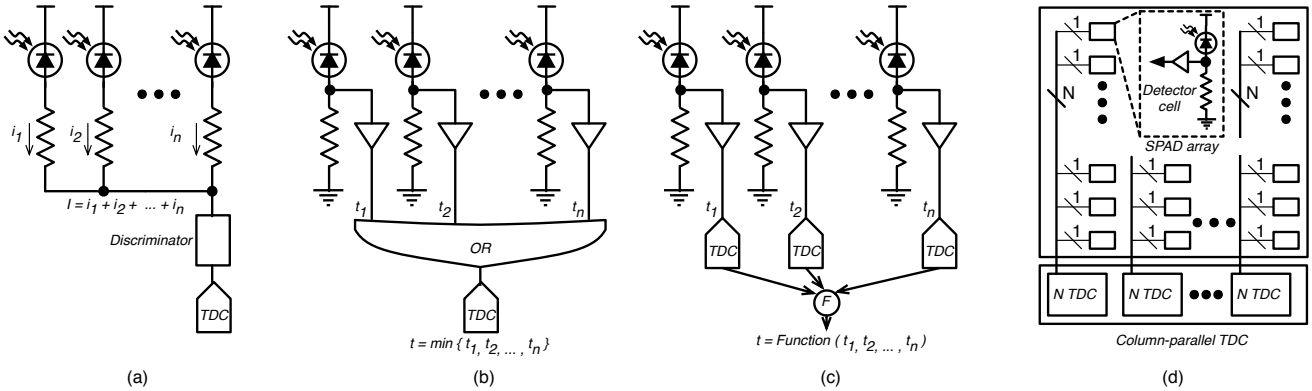

Fig. 1. The concept of (a)Analog SiPM, (b)Conventional Digital SiPM, (c)Ideal multi-channel digital SiPM and (d) Proposed Multi-Digital SiPM

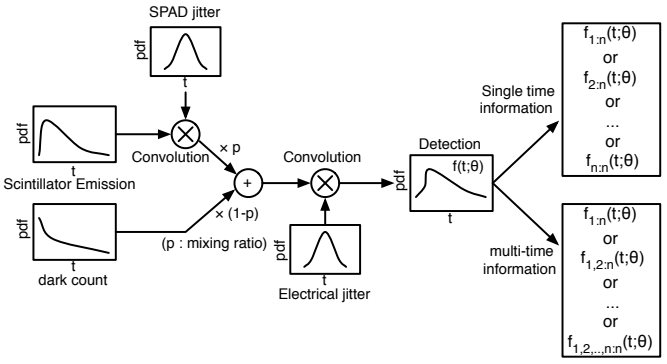

Fig. 2. Method for calculating the probability distribution function for the emission from scintillator and DCR.

Finally, the mixed pdf is used for calculating Fisher information [14] for the rth-order statistics pdf or the joint pdf for the first r-order statistics, then the Crámer-Rao lower bound for the unbiased estimator, θ is calculated. This procedure is shown in Fig. 2.

B. Simulation Results

For our simulations, we assumed normal SPAD jitter and electrical jitter distributions with a standard deviation of 100 ps, the rise and decay times of a LYSO scintillator are 200 ps and 40 ns, respectively, while the number of detected photons is varied from 100 to 5000, and DCR is varied from 1 Hz to 100 MHz. Fig. 3 shows the relation between order statistics and full-width-at-half-max (FWHM) timing resolution. Fig. 3 (a) shows that the timing resolution improves with multiple timestamps. Furthermore, the timing resolution with multiple timestamps doesn't degrade due to DCR while the timing resolution with a single timestamp degrades with certain amount of DCR, as shown in Fig. 3 (b). Fig. 4 (a) and 5 (a) summarize the relation between the number of detected photons and timing resolution using a single timestamp and multiple timestamps. The FWHM with multiple timestamps improves 13% if compared to the FWHM with a single timestamp at less than 100 kHz DCR, however, the FWHM is 20% and 40% better at 1 MHz and 10 MHz DCR, respectively. The rank(s) of the optimal estimator for a single timestamp and multiple timestamps in each number of detected photons are also shown in Fig 4 (b) and 5 (b). Fig. 6 (a) shows the timing resolution dependency on signal-to-noise ratio of number of the detected photons and DCR with different frame periods. The results show that multiple timestamps can still maintain the some time resolution with worse SNR while more time stamps are needed. Shorter frame periods reduce the required order statistics to give the minimum timing resolution as shown in Fig. 6 (b). From this work, it is clear that D-SiPMs capable of providing multiple timestamps are useful not only to improve timing resolution but especially to ensure tolerance to DCR and independence from a threshold. The proposed MD-SiPM is considered to be a promising architecture, as it achieves a good trade-off between detection robustness and timing resolution, thanks to a high overall fill factor.

III. Implementation and Measurement

A. Chip fabrication

Figure 7 shows the chip microphotograph, which includes an array of 4 $\times$ 4 MD-SiPMs, a row address decoder, MASKDATA and ENERGY registers, and a row of 192 TDCs. The MASKDATA register is used for disabling those pixels with DCR exceeding a threshold, so as to minimize spurious TDC activation. The ENERGY register is used for reading out the number of pixels that detected at least a photon. An independent SiPM readout (not shown in the picture) was implemented for testing purposes. Each SiPM and its fill factor are shown in the figure. A detail of the SiPM 'D15' is shown in the figure, along with the dimensions of the pixel that achieve a fill factor of 57%. To maximize fill factor, the electronics was placed at a distance of twice the pitch and implemented in a mirrored fashion. The cross-section and a detail of the SPADs, whereby deep well sharing was extensively used in the cathode.

B. Noise and sensitivity characterization

Figure 8 (a) shows cumulative DCR plot for 'D15' SiPM showing the DCR distribution of 416 SPADs for several excess bias voltages and temperatures. Masking pixels reduces both DCR and fill factor, and thus PDE, defined as $PDP \times FF$, where PDP is the photon detection probability and FF the

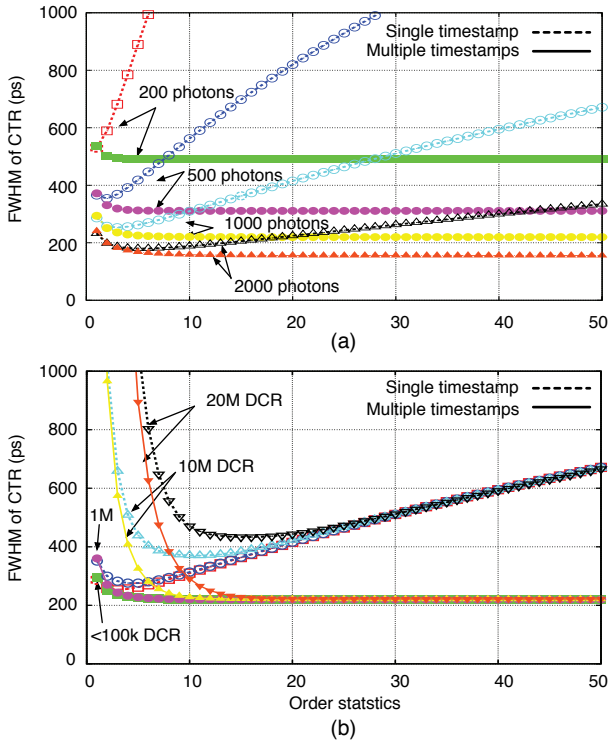

Fig. 3. Order statistics with a single timestamp or multiple timestamps v.s. FWHM of timing resolution: (a) various number of detected photons, 200, 500, 1000, and 2000 at 1 Hz DCR (which is almost negligible), (b) various values of DCR, less than 1MHz, 10MHz, 20MHz at 1000 detected photons.

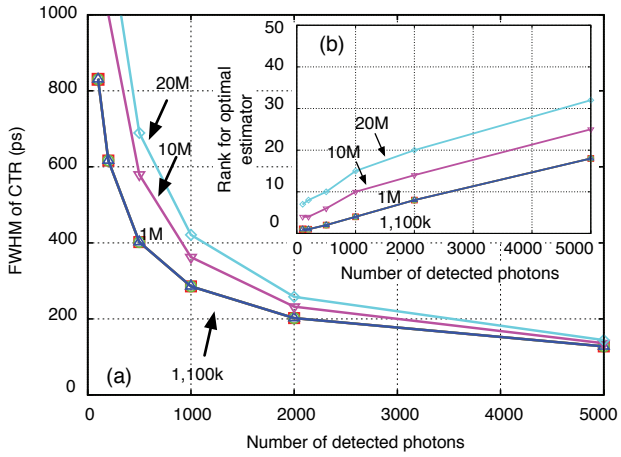

Fig. 4. (a) FWHM timing resolution v.s. number of detected photons using a single timestamp. (b) Rank of the optimal estimator.

fill factor. However, the reduction is not linear because some pixels have very high DCR compared to the median DCR value. Thus, small masking levels reduce DCR faster than PDE, while larger masking has a larger impact on PDE and a smaller impact on DCR. This mechanism can be seen in Figure 8 (b).

C. Timing characterization

The TDCs were fully characterized using an electrical input, yielding a single-shot timing uncertainty of 60 ps (FWHM).

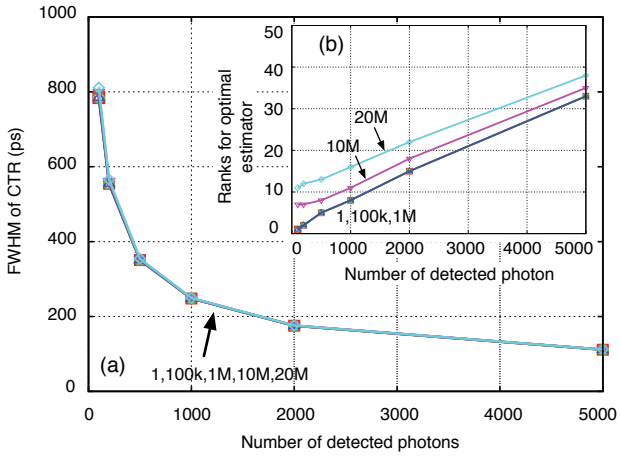

Fig. 5. (a) FWHM timing resolution v.s. number of detected photons using multiple timestamp. (b) Ranks of the optimal estimator.

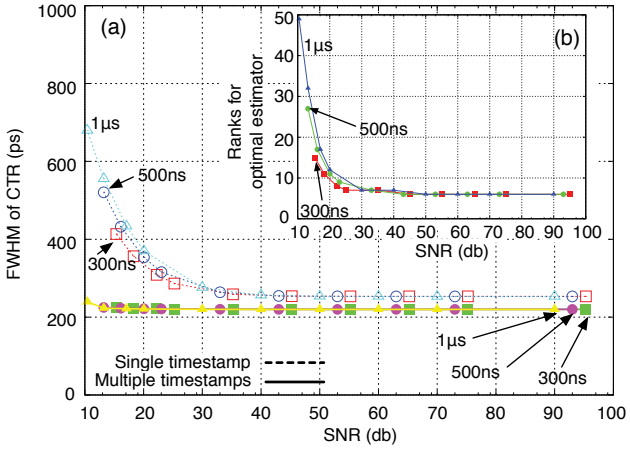

Fig. 6. Signal-to-noise ratio of number of detected photons and DCR with different frame period v.s. (a) FWHM of timing resolution using multiple timestamps, (b) Ranks of the optimal estimator.

The TDCs suffer from a 6 % to 9 % LSB shift in the ±30 °C range and ± 10 % power supply variation. The timing resolution of each SiPM was established optically in a TCSPC experiment using a 250 mW, 405 nm laser source (ALDS GmBH) with 40 ps pulse width and an external oscilloscope (LeCroy WaveMaster 6200) as shown in Figure 9 (a). A neutral density filter is used for reducing the power from the laser source to be single photon regime. The TCSPC experiment was repeated using the internal TDCs operating at a nominal LSB of 44 ps. A single-SPAD timing jitter (FWHM) of 121 ps was measured with internal TDCs and confirmed by the oscilloscope, as illustrated in Figure 9 (b). The timing jitter of the entire SiPM (all 416 pixels) was measured using the internal TDCs, yielding a single-shot timing jitter as low as 179 ps (FWHM) at 3.0 V excess bias, as shown in Figure 9 (c). This measurement is the sum in quadrature of the contributions from the intrinsic jitter of the SPADs, TDCs, and sensor skews.

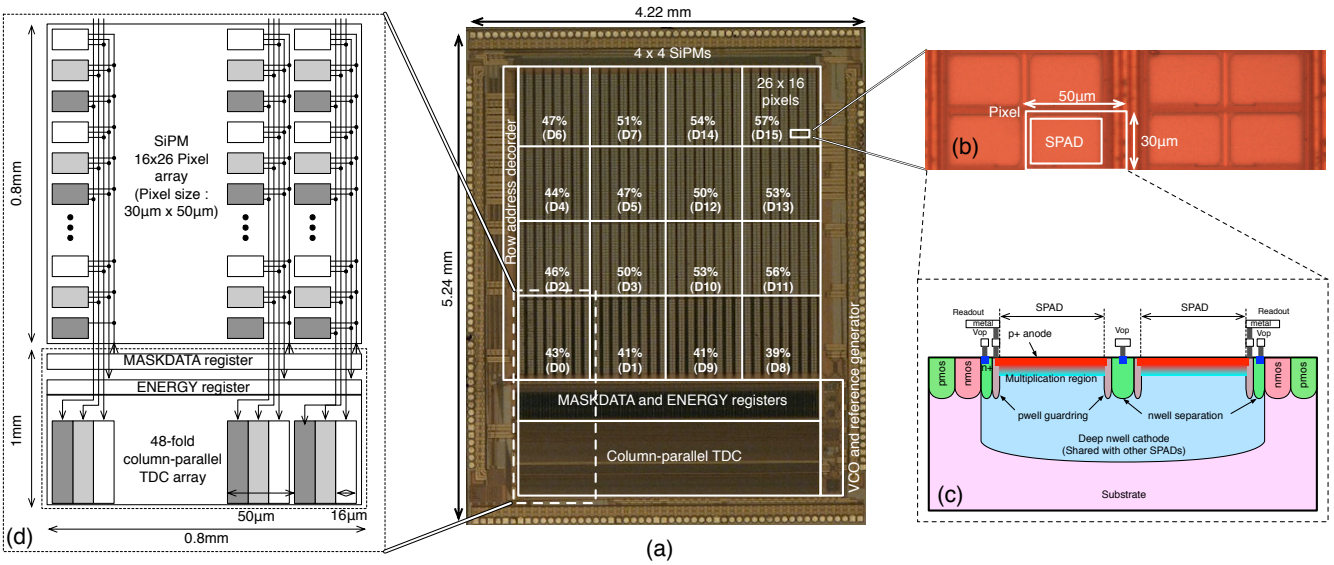

Fig. 7. (a) Chip microphotograph. The chip occupies an area of 22.1 mm^2 with a sensitive area of 3.2 × 3.2 mm^2. (b) Microphotograph focused on pixels. (c) The cross-section and a detail of the pixels. (d) The wire connections between pixels and the column-parallel TDCs. Adjacent pixels are routed to independent TDCs by triples; this approach prevents closely striking photons to be missed, thereby reducing local saturation.

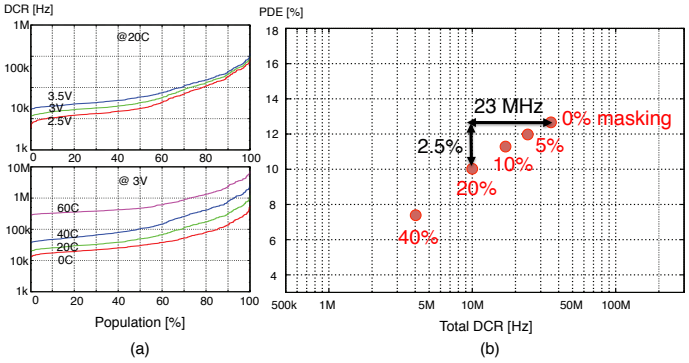

Fig. 8. (a) Cumulative DCR plot with various excess bias voltages and temperature for the 'D15' SiPM. (b) The relation between DCR and PDE for various SiPMs at 3 V excess bias and 20 °C.

IV. Conclusion

We have presented a comprehensive statistical analysis of timing resolution of a D-SiPM including the effect of PDE, DCR and electrical jitter with a LYSO crystal when multi timestamp is available. Simulation results show that D-SiPMs utilizing multiple timestamps (Multi-channel D-SiPM or MD-SiPM) can be more tolerant to DCR than those utilizing a single timestamp. The timing resolution is 13%, 20% and 40% better at 1000 detected photons, 200 ps rise time and 40 ns decay time of a LYSO scintillator, without DCR, with 1 MHz DCR and with 10 MHz DCR, respectively. Based on these findings, we have proposed new architectures to acquire multiple timestamps without sacrificing fill-factor. We also include the implementation and characterization of 4 × 4 MD-SiPMs coupled with an array of 44ps LSB TDCs for coincidence detection of gamma rays. The pitch of the SiPMs is 800 µm and the number of pixels in one SiPM is 416. The pixel has a 57 % fill factor with 121 ps timing resolution for a single photon. The SiPM timing resolution for single photon detection is 179 ps FWHM.

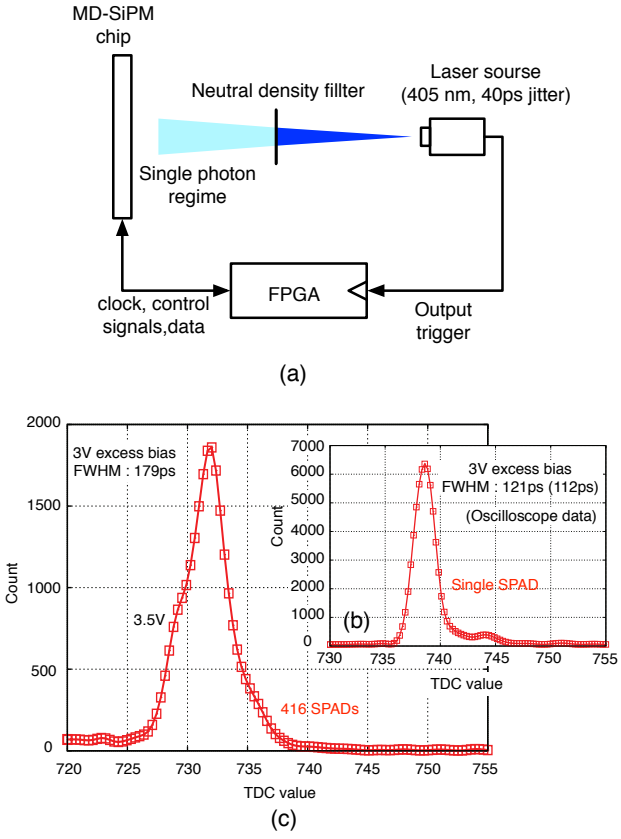

Fig. 9. (a) TCSPC experiment setup using a 250 mW, 405 nm laser source with 40 ps pulse width. (b) Single-photon FWHM timing resolution for a single SPAD using a TDC and an external oscilloscope. (c) Single-photon FWHM timing resolution for the complete SiPM at various excess bias voltages.

REFERENCES

[1] EndoTOFPET-US Proposal, Novel multimodal endoscopic probes for simultaneous PET/ultrasound imaging for image-guided interventions, European Union 7^{th} Framework Program (FP7 / 2007-2013) under Grant Agreement No. 256984, Health-2010.1.2-1.

[2] E. Garutti, "Endotofpet-us a novel multimodal tool for endoscopy and positron emission tomography," in *Proc. IEEE Nuclear Science Symp. Conf.*, 2012.

[3] MPPC, http://jp.hamamatsu.com.

[4] P. Buzhan, B. Dolgoshein, L. Filatov, A. Ilyin, V. Kantzerov, V. Kaplin, A. Karakash, F. Kayumov, S. Klemin, E. Popova, and S. Smirnov, "Silicon photomultiplier and its possible application," *Nucl. Instrum. Methods Phys. Res. A*, vol. 504, no. 1-3, pp. 48–52, 2003.

[5] A. G. Stewart, V. Saveliev, S. J. Bellis, D. J. Herbert, P. J. Hughes, and J. C. Jackson, "Performance of 1-mm^2 silicon phopomultiplier," *IEEE J. Quantum Electron.*, vol. 44, no. 2, pp. 157–164, Feb. 2008.

[6] N. Zorzi, M. Melchiorri, A. Piazza, C. Piemonte, and A. Tarolli, "Development of large-area silicon photomultiplier detectors for PET applications at FBK," *Nucl. Instrum. Methods Phys. Res. A*, vol. 636, no. 1, pp. 208–213, 2010.

[7] M. Mazzillo, G. Condorelli, D. Sanfilippo, G. Valvo, B. Carbone, A. Piana, G. Fallica, A. Ronzhin, M. Demarteau, S. Los, and E. Ramberg, "Timing performances of large area silicon photomultipliers fabricated at STMicroelectronics," *IEEE Trans. Nucl. Sci.*, vol. 57, no. 4, pp. 2273–2279, Aug. 2010.

[8] M. McClish, P. Dokhale, J. Christian, C. Stapels, E. Johnson, R. Robertson, and K. S. Shah, "Performance measurements of CMOS position sensitive solid-state photomultipliers," *IEEE Trans. Nucl. Sci.*, vol. 57, no. 4, pp. 2280–2286, Aug. 2010.

[9] T. Frach, G. Prescher, C. Degenhardt, R. Gruyter, A. Schmitz, and R. Ballizany, "The digital silicon photomultiplier principle of operation and intrinsic detector performance," in *Proc. IEEE Nuclear Science Symp. Conf.*, 2009, pp. 1959–1965.

[10] C. Veerappan, J. Richardson, R. Walker, D. U. Li, M. Fishburn, Y. Maruyama, D. Stoppa, F. Borghetti, M. Gersbach, R. K. Henderson, and E. Charbon, "A 160 $\times$ 128 single-photon image sensor with on-pixel 55 ps 10b time-to-digital converter," in *IEEE ISSCC Dig. Tech. Papers*, 2011, pp. 312–314.

[11] M. W. Fishburn and E. Charbon, "System trade-offs in gamma-ray detection utilizing SPAD arrays and scintillators," *IEEE Trans. Nucl. Sci.*, vol. 57, no. 5, pp. 2549–2557, Oct. 2010.

[12] S. Seifert, H. T. van Dam, and D. R. Schaart, "The lower bound on the timing resolution of scintillation detectors," *Phys. Med. Biol.*, no. 57, pp. 1797–1814, 2012.

[13] J. Glodo, W. Moses, W. Higgins, E. van Loef, P. Wong, S. Derenzo, M. Weber, and K. Shah, "Effects of ce concentration on scintillation properties of labr$_3$:ce," *IEEE Trans. Nucl. Sci.*, vol. 52, no. 10, pp. 1805–1808, Oct. 2005.

[14] S. Park, "On the asymptotic fisher information in order statistics," *Metrika*, vol. 57, no. 1, pp. 71–80, 2003.